Measured Constraints on Cloud-Top Entrainment to Reduce Uncertainty of Non-Precipitating Stratocumulus Shortwave Radiative Forcing in the Southern Ocean

K. J. Sanchez[1*], G. C. Roberts[1,2], M. Diao[3], and L. M. Russell[1]

[1]Scripps Institution of Oceanography, University of California, San Diego, CA, USA
[2]Centre National de Recherches Météorologiques, Météo-France & CNRS UMR3589, Toulouse, France
[3]Department of Meteorology and Climate Science, San Jose State University, San Jose, CA, USA

Corresponding author: Kevin Sanchez (kjsanche@ucsd.edu)

*Now at: Universities Space Research Association, Columbia, MD, USA
Now at: NASA Langley Research Center, Hampton, VA, USA

Key Points:

- Basic vertical profile measurements are sufficient to constrain entrainment in non-precipitating Southern Ocean (SO) stratocumulus clouds
- The sensitivity of shortwave cloud forcing to entrainment is 2-20 times the sensitivity to particle concentration or cloud-base updraft
- Quantifying the impact of entrainment on shortwave cloud forcing is needed to determine the energy budget in the SO

Abstract

Stratocumulus cloud-top entrainment has a significant effect on cloud properties, but there are few observations quantifying its impact. Using explicit 0D parcel model simulations, initialized with below-cloud in-situ measurements, and validated with in-situ measurements of cloud properties, the shortwave cloud radiative forcing (SWCF) was reduced by up to 100 W m^{-2} by cloud-top entrainment in the Southern Ocean. The impact of entrainment-corrected SWCF is between 2 and 20 times that of changes in the aerosol particle concentration or updraft at cloud base. The variability in entrainment-corrected SWCF accounts for up to 50 W m^{-2} uncertainty in estimating cloud forcing. Measurements necessary for estimating the impact of entrainment on cloud properties can be constrained from existing airborne platforms and provide a first-order approximation for cloud radiative properties of non-precipitating stratocumulus clouds. These measurement-derived estimates of entrainment can be used to validate and improve parameterizations of entrainment in Global Climate Models.

Plain Language Summary

Clouds over the ocean have a significant impact on climate because they reflect sun light that would otherwise be absorbed by the ocean. Understanding and accurately modeling how much sunlight these clouds reflect is important to understand feedbacks between clouds and climate. Using a simple model and cloud measurements, mixing of moist cloud air with warm-dry air from above the cloud was shown to decrease the cloud droplet number concentration and consequently total liquid water, which significantly decreases the overall amount of sunlight reflected by the cloud. Cloud droplets form onto small particles as they enter the base of the cloud through an updraft, in the meantime, warm-dry air from above the cloud mixes downward. In this study, the warm-dry air from above the cloud was shown to be more influential on reflecting sunlight than the concentration of particles and the updraft velocity at cloud-base. These results emphasize the importance of accurately accounting for the mixing in of warm-dry air from above the cloud in climate models, and can be constrained by existing measurements that are readily available on weather balloons and aircraft.

1 Introduction

Low clouds in the Southern Ocean (SO) are poorly simulated by general circulation models (GCMs) and tend to overestimate the amount of radiation absorbed by the SO (Bodas-Salcedo et al., 2014; Haynes et al., 2011; Hyder et al., 2018; McCoy et al., 2014). This bias is driven by underestimates of cloud radiative forcing, which are likely due to errors in cloud microphysical properties such as droplet size and concentration, as well as cloud processes such as precipitation and entrainment (Mason et al., 2015; Vial et al., 2013). Cloud properties in the SO are also particularly sensitive to aerosol loading due to relatively low background aerosol concentrations (Downey et al., 1990; Whittlestone & Zahorowski, 1998). Therefore, addressing these uncertainties is necessary for assessing future climate change feedbacks. GCM shortcomings, biases in satellite retrievals, and the scarcity of SO cloud measurements (Lenschow et al., 1999; Russell et al., 1998; Seinfeld et al., 2016) motivated the Southern Ocean Clouds, Radiation, Aerosol Transport Experimental Study (SOCRATES), which conducted in-situ airborne measurements of clouds, aerosol, and meteorological state over the SO on the NSF/NCAR HIAPER Gulfstream V (GV) (Laursen et al., 2006). The analysis shown here aims to improve GCM estimates of reflected shortwave radiation and the earth's energy budget by

obtaining measurements of cloud top entrainment drying with widely used measurements to improve the parameterization of clouds in models.

Aerosol-cloud interactions account for a significant part of the uncertainty in the global energy budget (IPCC, 2014; Lohmann, 2017; Nazarenko et al., 2017; Seinfeld et al., 2016; Stevens, 2015). Variability in reflected shortwave radiation (or albedo) is caused by differences in cloud fraction, cloud optical thickness, cloud droplet number concentration (CDNC) and cloud lifetime (Albrecht, 1989; Jiang et al., 2006; M. Wang et al., 2012). Aerosol indirect effects such as enhancements in particle concentrations leading to increased CDNC and increased reflected solar radiation are classic examples of how changes in particle concentrations alter cloud optical properties (Ackerman et al., 2000; Albrecht, 1989; Jiang et al., 2006; Lu & Seinfeld, 2005; Twomey, 1977; Xue & Feingold, 2006). While correctly representing CDNC is a concern in GCMs for accurately modeling the optical thickness of clouds, uncertainty in liquid water path (LWP) accounts for more than a factor of two change in cloud optical thickness compared to CDNC (Brenguier et al., 2011), making LWP of first-order importance (Boers & Ross, 1994; Lu et al., 2008). One of the biggest factors in determining marine stratocumulus LWP is the cloud-top entrainment rate, however, numerous feedbacks between the cloud properties and entrainment make simulating and parameterizing entrainment rates challenging (Chen et al., 2011). Even though cloud-top entrainment and detrainment play an important role in the resulting cloud optical properties, their roles in determining cloud optical properties are not often considered in aerosol-cloud closure studies.

Entrainment of free tropospheric air at cloud top typically results in a warmer, drier boundary layer, as well as, clouds with subadiabatic LWP and decreased precipitation (Ackerman et al., 2009; Chen et al., 2011; Deardorff, 1980; Hill et al., 2009; Lu & Seinfeld, 2005; Wood, 2007; Xue & Feingold, 2006). Under certain thermodynamic conditions, when the above-cloud entrained air is excessively dry, the air mixture can result in a parcel becoming negatively buoyant due to evaporative cooling, leading to enhancements in the entrainment rate (Ackerman et al., 2004; Burnet & Brenguier, 2007; Grabowski, 1993). The exchange of air between cloud top and the overlying air is determined by the gradient in specific humidity and temperature across the inversion (Sanchez et al., 2017; Stevens, 2002), both of which are expected to change in a warming climate (Qu et al., 2015). Increased temperature gradients between the marine boundary layer (MBL) and free troposphere, result in stronger inversions

which decrease cloud-top entrainment rates (Ackerman et al., 2004; Caldwell & Bretherton, 2009) and increase cloud fraction (Caldwell et al., 2013). However, enhanced specific humidity gradients across the inversion (Webb & Lock, 2013) also lead to increased evaporation-driven entrainment at cloud-top, which thins stratocumulus clouds in LES simulations (Bretherton, 2015; Bretherton et al., 2013).

Cloud top entrainment is also affected by an aerosol-driven feedback on the entrainment rate. For example, a decrease in aerosol loading leads to larger cloud droplets and an enhancement in droplet sedimentation and precipitation at cloud top, which results in a decrease in cloud-top LWC, and consequently, a decrease in evaporative cooling and entrainment as well (Bretherton, 2015; Bretherton et al., 2007; Turton & Nicholls, 1987; Zuidema et al., 2008). Large Eddy Simulation (LES) by Zuidema (2008) show increased particle concentrations are linked to decreased cloud fraction as a result of more entrainment in spite of less drizzle. Further complicating this process, cloud-top entrainment is initiated by mixing on centimeter to meter length scales, meaning it cannot be explicitly resolved in LES models or GCMs, requiring entrainment to be a parameterized process. In previous LES studies of stratocumulus clouds, the vertical resolution has been increased in an attempt to reduce the uncertainty in the entrainment rate and resulted in a decrease in the over-prediction of cloud-top entrainment, and consequently, under-predicting the cloud radiative forcing (Bretherton et al., 1999; Stevens et al., 2005). In addition, Stevens et al., (2005) found that increasing the horizontal resolution is important for resolving the strength of large eddies (> 70 m), and hence, improves the calculation of the entrainment rate.

In GCMs, the Cloud Layers Unified by Binormals (CLUBB) parameterization is the most promising method of reproducing sub-grid-scale cloud properties and involves using probability distribution functions (PDF) derived from sub-grid scale predictive moments to derive cloud properties over multiple regimes (Guo et al., 2010, 2014). GCMs are constrained with satellite measurements; however, current satellite-derived cloud properties assume a 30% reduction in CDNC due to inhomogeneous entrainment (Rosenfeld et al., 2016). Entrainment drying in the CLUBB parameterization can be tuned, and the mixing line approach from this study can be utilized to obtain datasets for improving entrainment in the CLUBB parameterization (Guo et al., 2014).

In this manuscript, five case studies are used to quantify the impact of cloud-top entrainment on stratocumulus cloud optical properties in the SO using a concept first described by Betts (1983) and Paluch (1979). Betts (1983) showed that stratocumulus clouds largely follow a mixing line structure from cloud-base to cloud-top, where conservative variables are linearly related, indicating that entrained air at cloud-top vertically mixes throughout the cloud. This concept was recently utilized by Sanchez et al. (2017) and Calmer et al. (2019) to account for entrainment-induced evaporation of cloud droplets which improved representation of non-precipitating stratocumulus cloud optical properties. The method used in a pristine mid-latitude marine environment (Sanchez et al., 2017) and a polluted Mediterranean region (Calmer et al., 2019) is also verified for SO clouds during the SOCRATES experiment. By combining in-situ measurements of cloud condensation nuclei (CCN) spectra at cloud base, vertical profiles of the thermodynamic properties throughout the marine boundary layer, updraft and an aerosol-cloud-parcel model (ACPM), this study obtains accurate simulations of the observed cloud optical properties by incorporating the impact of entrainment on the microphysical properties of stratocumulus clouds in the SO. We also relate the sensitivity of stratocumulus shortwave cloud forcing (SWCF) to changes in below-cloud aerosol concentrations and updraft, as well as to the impact of entrainment (ENT_{LWC}, Sections 2.4) via the reduction of liquid water path (LWP). The mixing-line entrainment approximation ($ENT_{ML,}$ Sections 2.5 and 3.2) enables the calculation of the entrained fraction of air and resulting sub-adiabatic LWC throughout the cloud using only vertical profiles of temperature, pressure and relative humidity measurements. This technique to account for entrainment can eventually be applied globally to non-precipitating stratocumulus clouds using relatively simple observations to constrain and evaluate GCM parameterizations.

2 Methods

2.1 NSF/NCAR HIAPER GV measurements

Measurements used in SOCRATES are collected on the NSF/NCAR Gulfstream-V High-performance Instrumented Airborne Platform for Environmental Research (GV HIAPER) observational platform. The GV was stationed at the Hobart International Airport, Tasmania, during the austral summer between 15 January and 24 February 2018. The flight strategy during SOCRATES involved ferrying out to an area of interest followed by a series of straight vertical profiles, and level legs to sample below, in and above cloud in the marine boundary layer. The

GV conducted 15 research flights (RF) over the SO between 42.5 °S and 62.1 °S and between 133.8 °E and 163.1 °E at altitudes ranging from 50-7500 m.

A wing-mounted Ultra-High Sensitivity Aerosol Spectrometer (UHSAS, DMT, Boulder, CO) measured particle size distribution between 0.06 and 1.0 μm in diameter; however the 0.6-0.7 μm bins were not used due to instrument noise at these sizes. A condensation particle counter (CPC, TSI 3760A) was used to measure total particle concentrations (N_p, diameter > 10 nm). CCN measurements were performed with two miniature continuous-flow stream-wise thermal gradient chambers, one in scanning supersaturation mode and one in constant supersaturation mode (Roberts & Nenes, 2005). The supersaturation range in the scanning CCN counter spanned from 0.06-0.87 % and a single spectrum recorded every five minutes. The constant supersaturation CCN counter operated at 0.43 % supersaturation, at 1 Hz. The internal chamber pressure of both CCN counters was controlled to 400 hPa. Updraft distributions at cloud base were measured by the GV HIAPER Cloud Radar (HCR), corrected for plane orientation with nadir looking data. HCR reflectance and a Particle Habit Imaging and Polar Scattering probe (Abdelmonem et al., 2016; Schnaiter et al., 2018) were also used to identify clouds without drizzle (Chin et al., 2000; Kato et al., 2001; Kogan et al., 2005). A high frequency (25 Hz) Vertical Cavity Surface Emitting Laser (VCSEL) water vapor hydrometer was used to measure the water vapor mixing ratio (Zondlo et al., 2010). A QA/QC water vapor dataset at 25 Hz for the SOCRATES campaign (Diao, 2020) is further used to derive specific humidity (q_v) and relative humidity with respect to liquid (RH_{liq}). Finally, a cloud droplet probe (CDP, DMT, Boulder, CO) is used to measure cloud droplet concentration and size (2-50 μm diameter) to calculate liquid water content (LWC) and cloud droplet extinction for comparison with the ACPM (section 2.2).

2.2 Aerosol Cloud Parcel Model (ACPM) description

A 0D ACPM was used in this study because 1) it enables the simulated results to be constrained by measured thermodynamic properties, aerosol number size distributions, and CCN spectra (Table 1, Supporting Figure S1); and 2) the ACPM allows explicit comparison to in-situ measurements of cloud droplet size distributions (rather than parameterized cloud droplet size distributions used in LES). The ACPM is based on a fixed-sectional approach to represent the dry particle size domain, with internally-mixed chemical components. The model employs a

dual-moment (number and mass) algorithm (Tzivion et al., 1987) to calculate particle growth from one size section to the next for non-evaporating compounds (namely, all components other than water) using an accommodation coefficient of 1.0 (Raatikainen et al., 2013). Liquid water is treated in a moving-section representation, similar to the approach of Jacobson et al. (1994), to account for evaporation and condensation of water in conditions of varying humidity. The model includes a dynamic scheme for activation of particles to cloud droplets (Seinfeld & Pandis, 2006). Aerosol hygroscopicity was calculated using the UHSAS particle size distribution, CCN spectra and κ-Köhler theory (Kohler, 1936; Petters & Kreidenweis, 2007) in below-cloud samples by matching cumulative UHSAS distributions with CCN concentrations at all sizes above 70 nm diameter. The hygroscopicity of particles below 70 nm was considered to be the same as the calculated hygroscopicity at 70 nm. The CPC concentration and cumulative particle number distribution from the UHSAS were used to linearly interpolate particle concentrations between 10 and 70 nm diameter. In subsaturated conditions (i.e., relatively humidity < 100%), aerosol particles below the cloud base are considered to be in local equilibrium with water vapor pressure. A detailed description of the Aerosol Cloud Parcel Model (ACPM) is presented in Russell and Seinfeld (1998) and Russell et al. (1999). The criteria for selecting case studies is discussed in Supporting text S1.

The ACPM in-cloud lapse rate is adiabatic, and ultimately compared to observations to assess entrainment (Sections 2.4 and 2.5). A weighted ensemble of positive vertical velocities (Supporting Figure S1a) measured with the NCAR/NSF GV HIAPER cloud radar were applied to the ACPM to produce the simulated cloud droplet distribution (Sanchez et al., 2016). The shortwave cloud forcing (SWCF) is calculated as SWCF = αQ, where Q is the day average solar insolation (Table 1) based on the latitude and α is the cloud albedo which is derived from the vertical profile of the in-situ (CDP) and simulated (ACPM) cloud droplet size distribution and an asymmetric scattering parameter of 0.85 (see Supporting text S2) (Bohren & Battan, 1980; Geresdi et al., 2006; Hansen & Travis, 1974; Sanchez et al., 2017; Stephens, 1978). Coagulation, scavenging, and deposition of the aerosol were included in the ACPM, but their effects are negligible given the relatively short simulations used here (< 1 h), and their relatively low marine total aerosol particle concentrations (< 1000 cm^{-3}) and cloud LWC (< 1 g m^{-3}). As stated previously, cloud droplet sizes were < 20 μm diameter (for all but one case ($RF10_{Thick}$; Table 1),

therefore, autoconversion and accretion rates are not included in this simulation and exert a negligible effect on the simulated values of LWC and CDNC (Feingold et al., 2013).

2.3 ACPM cloud-top entrainment

The process of entrainment and its effect on a cloud can be described as the weighted downward mixing of above-cloud warm, dry air into the cloudy air below causing cloud droplets to evaporate. This air-parcel, subsequently mixes downward, diluting the cloud droplet concentration throughout the cloud, resulting in a reduction in CDNC compared to an adiabatic profile (Chen et al., 2011; S. Wang et al., 2003; Xue & Feingold, 2006). Five cases are available from this campaign to illustrate the effect of entrainment on SWCF in the SO (Table 1). These five cases are from four different research flights (RF) and are referred to by their flight number, with the two RF10 cases being differentiated by subscripts that describe the cloud thickness ($RF10_{Thin}$ or $RF10_{Thick}$). Simulated cloud profiles are produced using the ACPM using adiabatic conditions, which are then compared to in-situ observations and corrected for cloud-top entrainment.

2.4 Entrainment Derived from Liquid Water Content (ENT_{LWC})

The relative difference between simulated and observed values of LWC (or LWP) is related to the entrained fraction of above-cloud air. To account for the decrease in LWC associated with entrainment, the CDNC in the ACPM is decreased until the simulated (ACPM) and observed (CDP) LWC vertical profiles are the same. This approximation assumes inhomogeneous mixing, meaning only a fraction of the cloud droplets evaporate, whereas homogenous mixing implies all cloud droplets partially evaporate. Inhomogeneous mixing is consistent with past studies of well-mixed, non-precipitating stratocumulus clouds (Brenguier et al., 2011; Burnet & Brenguier, 2007; Jia et al., 2019). Furthermore, homogeneous mixing would not sufficiently account for the observed decrease in SWCF and CDNC. In this study, evaporation of droplets due to inhomogeneous mixing is independent of droplet size, therefore the volumetric mean diameter does not change due to droplet evaporation.

2.5 Entrainment Derived from a Mixing Line (ENT_{ML})

ENT_{ML} accounts for the sub-adiabatic LWC values due to cloud-top entrainment with inhomogeneous mixing, derived from temperature, pressure and q_v measurements. ENT_{ML}, first used by Sanchez et al. (2017) and Calmer et al. (2019), generates a mixing line (a linear

relationship between two conservative variables, Figure 1) between q_v at the cloud-base and above-cloud, and measurement-derived equivalent potential temperature (θ_E). q_v is equivalent to total water content (q_t), a conservative variable, in these subsaturated, non-precipitating conditions. With the mixing line, the in-cloud q_t is a function of θ_E, which is derived from in-cloud temperature, pressure and q_v (See Supporting text S3, Figure S3). The measured thermodynamic properties of the above-cloud air (shown as red squares in Figure 1) and cloud-base air are then used to estimate subadiabatic LWC profile (Calmer et al., 2019; Sanchez et al., 2017). In this analysis, a line is made between a point at the cloud base and each point above the cloud that is identified as 'entrained air' (red-bounded grey markers in Figure 1 and Supplemental Figure S4). Each line is used to calculate an entrainment-corrected vertical profile of CDNC, LWC, cloud droplet extinction and integrated SWCF. The solid black line in Figure 1 and 2 is the 50th percentile (median) of the CDNC, LWC and extinction, while the black dashed lines represent the 25th and 75th percentiles. See the Supporting text S3 and S4 for details on the measurements that represent the entrained air that are used to derive sub-adiabatic cloud liquid water content.

3 Results

The observed LWC profiles in the SO are sub-adiabatic (Figure 2b,f) for all cases studied during the SOCRATES experiment. CDNCs are also always lower than the adiabatic simulations (Table 1, Figure 2) while the volumetric diameter (D_v) is consistent with adiabatic simulations, suggesting entrainment of dry air is reducing LWC via the evaporation of cloud droplets. These results are consistent with previous observations in the SO (Yum et al., 1998), the tropics (Rauber et al., 2007; Roberts et al., 2008) and mid-latitudes (Calmer et al., 2019; Sanchez et al., 2017). Consequently, the SWCF and CDNCs above cloud-base are significantly and consistently overestimated compared to adiabatic conditions (Table 1).

3.1 ENT_{LWC}; comparison of ACPM to observations

To illustrate the impact of entrainment on cloud microphysical and optical properties, Figure 2 shows the vertical profiles of observed and simulated D_v, LWC, CDNC, and cloud droplet extinction for RF12 and $RF10_{Thick}$ to illustrate two distinctly different cases for which entrainment corrections may be applied. The adiabatic ACPM overestimates the observed LWC, CDNC, and cloud droplet extinction; however, D_v remains remarkably similar to observed

values, which supports evidence for inhomogeneous mixing (Brenguier et al., 2011; Burnet & Brenguier, 2007; Jia et al., 2019).

In-cloud level-legs that straddled the vertical profiles for RF02 and RF13 cases, shown in Supporting Figure S6 show LWC, CDNC, and D_v varied consistently together over tens of kilometers, suggesting that inhomogeneous mixing also remains consistent over tens of kilometers. The horizontal variability in-cloud properties corresponds to changes in the cloud base height, as shown by the downward facing HIAPER radar reflectivity during the RF13 in-cloud level-leg (Supporting Figure S7). By accounting for entrainment with ENT_{LWC} (Section 2.4), simulated CDNC and extinction reproduce observed values.

Table 1 shows the difference in SWCFs comparing observations to the adiabatic model ($\delta SWCF_{adiabatic}$) and accounting for entrainment using LWC ($\delta SWCF_{ENT_{LWC}}$) and mixing line ($\delta SWCF_{ENT_{ML}}$) corrections. A difference of 0 W m^{-2} implies adiabaticity. $\delta SWCF_{adiabatic}$ represents the upper limit and ranged from 38.4±8.9 to 93.4±17.1 W m^{-2}; while $\delta SWCF_{ENT_{LWC}}$ are significantly lower, between 5.3±16.2 and 32.1±14.2 W m^{-2}. As LWC in the observed and ENT_{LWC} vertical profiles are, by definition, the same, $\delta SWCF_{ENT_{LWC}}$ is greater than zero because of narrower droplet spectrum width and greater CDNC in the simulations. Compared to the adiabatic simulations, CDP-derived LWP was reduced by 28%-58% as a result of cloud-top entrainment. For these five cases, the range in SWCF associated with 28% and 58% reduction in LWP compared to an adiabatic LWP amounts to 53 W m^{-2} (Table 1). This implies that variability in entrainment exerts an uncertainty in radiative forcing of individual clouds up to 50 W m^{-2}.

The ACPM was used to further quantify and compare the sensitivity of SWCF and CDNC to changes in aerosol (N_p), updraft (w), and LWP related to entrainment (Table 1). In these sensitivity calculations, N_p and w distributions were evaluated at half and double their observed values (i.e., $0.5N_p$ and $2N_p$; $0.5w$ and $2w$). Table 1 shows that SWCF is 2-4 times more sensitivity to N_p than w over the SO. Similarly, CDNC was approximately 1-3 times more sensitive to N_p than w. This indicates that clouds in the SO form in an aerosol-limited regime, which is characteristic of the marine boundary layer (Reutter et al., 2009; Sanchez et al., 2016). Table 1 shows that the SWCF sensitivity to entrainment and subsequent reduction of LWP are 2-20 times those related to N_p and w. CDNC is approximately twice as sensitive to entrainment

compared to N_p and up to four times more sensitive than the updraft. This highlights the first-order role of entrainment in determining cloud microphysical properties.

The SWCF for RF02 and $RF10_{thick}$ illustrate limiting cases in this study as they are the most and least sensitive, respectively, to both N_p and entrainment. The RF02 SWCF case shows the greatest sensitivity to N_p and entrainment because it has the lowest CDNC concentration and it is the thinnest cloud of the five cases ($\delta SWCF_{ENT_{LWC}}$= 32.1±14.2 W m^{-2}; Table 1). In contrast, the impact of entrainment on $RF10_{Thick}$ is lower than the other cases in this study because the cloud is significantly thicker (Table 1), and the cloud SWCF is less sensitive to changes in optical thickness when the optical thickness is high (Sanchez et al., 2016) (Supporting Figure S8). The $RF10_{Thick}$ case is also unique relative to the other cases because it has a large Aitken mode, as well as the highest CCN concentration (Supporting Figure S1c, Table 1). The $RF10_{Thick}$ CDNC is more sensitive to N_p than *w* (aerosol-limited case; Reutter et al., 2009); however, it is relatively more sensitive to *w* compared to the other cases in this study because of the high Aitken mode particle concentration (similar to findings by Sanchez et al. (2016)).

3.2 ENT_{ML}; comparison of ACPM to observations

Compensating SWCF for entrainment mixing using ENT_{ML} (Section 2.5) and ENT_{LWC} (Section 2.4) yield similar results (within ~ 15 W m^{-2}) for three out of the five cases of observations (Table 1). For RF10, compensating SWCF using ENT_{ML} yielded results within ~50 W m^{-2} ($RF10_{Thin}$ ($\delta SWCF_{ENT_{ML}}$= 54.2±16.2 W m^{-2}); $RF10_{Thick}$ ($\delta SWCF_{ENT_{ML}}$= 27.6±12.8 W m^{-2}; Table 1), showing only a relatively small improvement compared to $\delta SWCF_{adiabatic}$. The main limitation of ENT_{ML} results from discrepancies in the approximation of LWC (and LWP), as ENT_{ML} utilizes a linear relationship of q_t and θ_E (conservative variables) between the top and bottom of the cloud to calculate q_t as a function of the measurement-derived θ_E in the cloud. Since θ_E is a function of q_v and temperature, these two variables may co-vary, yet θ_E remains constant even while q_t may vary vertically in the cloud. In such a case, the ENT_{ML}-derived q_t would also be constant and represents an adiabatic limit. For example, $RF10_{Thick}$ shows a constant θ_E between cloud base (290 m) and ~600 m, which is also the same altitude as an in-cloud temperature inversion (Figure 1b, Supporting Figure S3d,i). As θ_E is constant, ENT_{ML}-derived q_t approaches the adiabatic limit even though the observed values of q_t decrease ~0.2 g kg^{-1} in this section of the cloud based on CDP observations (not shown). $RF10_{Thin}$ (Supporting

Figures S3 and S4) also has a nearly constant in-cloud θ_E, resulting in an overestimation of q_t (and LWP).

In summary, a constant in-cloud θ_E yields ENT_{ML}-derived q_t profiles that approach adiabatic LWP, CDNC and SWCF limits. Consequently, ENT_{ML} represents a minimum limit (but still substantial improvement) for assessing the impact of entrainment on non-precipitating cloud microphysical and radiative properties.

4 Discussion and Implications

This study uses in-situ measurements from the Southern Ocean Clouds, Radiation, Aerosol Transport Experimental Study (SOCRATES), collected on the NSF/NCAR HIAPER Gulfstream V (GV) during the austral summer. Measurements were used to assess the impact of cloud-top entrainment by combining in-situ observations of cloud condensation nuclei (CCN) spectra, aerosol number size distributions and updrafts at cloud base to initialize an aerosol-cloud parcel model (ACPM) and compare simulated cloud microphysical and optical properties to those derived by a cloud droplet probe (CDP). Differences in shortwave cloud forcing (SWCF) between adiabatic simulations and subadiabatic observations of a non-precipitating stratocumulus cloud layer in the SO resulted in values as high as ~100 W m^{-2}. SWCF was simulated to within 16 W m^{-2} using CDP-derived entrainment (ENT_{LWC}) for four of the five cases. In one of the cases (RF02), the difference between ENT_{LWC} and observed SWCF is relatively large due to the higher sensitivity of SWCF to particle concentrations. This case was also the thinnest cloud in this study, and SWCF sensitivity to entrainment is higher for such conditions (Supporting Figure S8).

Even when accounting for the impacts of entrainment on cloud optical properties, the entrainment-corrected LWP varied between 28%-58%, which translates to a range of 53 W m^{-2} in SWCF related to variability in entrainment for the cases studied here. For comparison, the sensitivity of SWCF due to entrainment is between 2 and 20 times the sensitivities of SWCF related to particle concentration and updraft – thus emphasizing the importance of accurately accounting for entrainment in climate models.

ENT_{ML} (mixing-line approach) was simulated to within 15 W m^{-2} except for two cases. ENT_{ML} utilizes the linear relationship of two conservative variables (total water content (q_t) and θ_E) to derive in-cloud q_t from the measured in-cloud θ_E to calculate the entrainment-induced

reduction in LWP. This method was first shown in pristine and polluted mid-latitude clouds (Calmer et al., 2019; Sanchez et al., 2017), and is now reproduced here with in-situ CDP measurements for clouds in the SO. ENT_{ML} only requires measurements of pressure, temperature, and relative humidity (PTU) in and above the cloud as well as the vertical extent of the cloud to estimate the sub-adiabatic LWC profile. ENT_{LWC} is certainly a more accurate method to account for entrainment, but also requires the deployment of a CDP (or similar instrument to measure CDNC and LWC), which is not nearly as ubiquitous as PTU measurements. PTU measurements can be obtained with numerous airborne platforms (i.e., radiosondes, aircraft and UAVs) as long as the vertical resolution is high enough to capture the temperature and water vapor immediately above the cloud layer (within ~10 to 100 meters).

ENT_{ML} approaches an adiabatic profile (i.e., no entrainment correction), if θ_E remains constant in the cloud while q_t actually varies. Nonetheless, ENT_{ML} could be used to improve GCM parameterizations, such as multivariate PDFs representing sub-grid-scale moisture, temperature and vertical velocity to derive cloud microphysical parameters across multiple cloud regimes (Guo et al., 2010). Reducing the uncertainty of cloud optical properties in GCM models remains a fundamental challenge for correctly representing the Earth's energy budget (Bretherton et al., 2013; Brient et al., 2019; Hourdin et al., 2015; de Szoeke et al., 2010). For decades now, the IPCC has reported an uncertainty in the anthropogenic-induced cloud forcing of approximately 1.5 W m^{-2}, which represents nearly 75% of the uncertainty related to the total anthropogenic radiative forcing (IPCC, 2014). This study in the SO extends beyond earlier studies in the mid-latitudes (Sanchez et al., 2016; Calmer et al., 2019) to show that the reduction in LWP owing to entrainment is a major contributor to uncertainty in SWCF for stratocumulus clouds globally. Improving the parameterizations of entrainment using the mixing line techniques presented here has the potential to significantly improve GCM representation of cloud optical properties and, ultimately, the Earth's energy budget.

Acknowledgments

K. J. Sanchez and G. C. Roberts acknowledge the support of NSF Grant No. AGS-1660374. M. Diao acknowledges the support of NSF AGS-1642291 and NSF OPP-1744965 grants, and the NCAR ASP Faculty Fellowship. SOCRATES data are available through the following EOL UCAR repository https://data.eol.ucar.edu/master_lists/generated/socrates/

(UCAR/NCAR-Earth Observing Laboratory, 2019b, 2019a; K. Sanchez & Roberts, 2018; UCAR/NCAR-Earth Observing Laboratory, 2018). The VCSEL water vapor QC/QA data can be accessed at https://data.eol.ucar.edu/dataset/552.052. The authors have no conflicts of interest to disclose. We thank the UCAR/NCAR-Earth Observing Laboratory and the flight crew for all the work done to obtain the measurements used in this manuscript.

References

Abdelmonem, A., Järvinen, E., Duft, D., Hirst, E., Vogt, S., Leisner, T., & Schnaiter, M. (2016). PHIPS-HALO: The airborne Particle Habit Imaging and Polar Scattering probe-Part 1: Design and operation. *Atmospheric Measurement Techniques*, *9*(7), 3131–3144. https://doi.org/10.5194/amt-9-3131-2016

Ackerman, A. S., Toon, O. B., Taylor, J. P., Johnson, D. W., Hobbs, P. V., Ferek, R. J., et al. (2000). Effects of Aerosols on Cloud Albedo: Evaluation of Twomey's Parameterization of Cloud Susceptibility Using Measurements of Ship Tracks. *Journal of the Atmospheric Sciences*, *57*(16), 2684–2695. https://doi.org/10.1175/1520-0469(2000)057<2684:EOAOCA>2.0.CO;2

Ackerman, A. S., Kirkpatrick, M. P., Stevens, D. E., & Toon, O. B. (2004). The impact of humidity above stratiform clouds on indirect aerosol climate forcing. *Nature*, *432*(7020), 1014–1017. https://doi.org/10.1038/nature03174

Ackerman, A. S., vanZanten, M. C., Stevens, B., Savic-Jovcic, V., Bretherton, C. S., Chlond, A., et al. (2009). Large-Eddy Simulations of a Drizzling, Stratocumulus-Topped Marine Boundary Layer. *Monthly Weather Review*, *137*(3), 1083–1110. https://doi.org/10.1175/2008MWR2582.1

Albrecht, B. A. (1989). AEROSOLS, CLOUD MICROPHYSICS, AND FRACTIONAL CLOUDINESS. *Science*, *245*(4923), 1227–1230. https://doi.org/10.1126/science.245.4923.1227

Betts, A. K. (1983). Thermodynamics of mixed stratocumulus layers: saturation point budgets. *Journal of the Atmospheric Sciences*, *40*(11), 2655–2670. https://doi.org/10.1175/1520-0469(1983)040<2655:TOMSLS>2.0.CO;2

Bodas-Salcedo, A., Williams, K. D., Ringer, M. A., Beau, I., Cole, J. N. S., Dufresne, J.-L., et al. (2014). Origins of the Solar Radiation Biases over the Southern Ocean in CFMIP2 Models*. *Journal of Climate*, *27*(1), 41–56. https://doi.org/10.1175/JCLI-D-13-00169.1

Boers, R., & Ross, M. M. (1994). Absorption feedback in stratocumulus clouds Influence on

427 cloud top albedo. *Tellus*, (0280–6495), 229–241.

428 Bohren, C. F., & Battan, L. J. (1980). Radar Backscattering by Inhomogeneous Precipitation
429 Particles. *Journal of the Atmospheric Sciences*, *37*(8), 1821–1827.
430 https://doi.org/10.1175/1520-0469(1980)037<1821:RBBIPP>2.0.CO;2

431 Brenguier, J. L., Burnet, F., & Geoffroy, O. (2011). Cloud optical thickness and liquid water
432 path-does the k coefficient vary with droplet concentration? *Atmospheric Chemistry and*
433 *Physics*, *11*(18), 9771–9786. https://doi.org/10.5194/acp-11-9771-2011

434 Bretherton, C. S. (2015). Insights into low-latitude cloud feedbacks from high-resolution models.
435 *Philosophical Transactions of the Royal Society A: Mathematical, Physical and*
436 *Engineering Sciences*, *373*(2054). https://doi.org/10.1098/rsta.2014.0415

437 Bretherton, C. S., Macvean, M. K., Bechtold, P., Chlond, A., Cotton, W. R., Cuxart, J., et al.
438 (1999). An intercomparison of radiatively driven entrainment and turbulence in a smoke
439 cloud, as simulated by different numerical models. *Quarterly Journal of the Royal*
440 *Meteorological Society*, *125*(554), 391–423. https://doi.org/10.1002/qj.49712555402

441 Bretherton, C. S., Blossey, P. N., & Uchida, J. (2007). Cloud droplet sedimentation, entrainment
442 efficiency, and subtropical stratocumulus albedo. *Geophysical Research Letters*, *34*(3),
443 L03813. https://doi.org/10.1029/2006GL027648

444 Bretherton, C. S., Blossey, P. N., & Jones, C. R. (2013). Mechanisms of marine low cloud
445 sensitivity to idealized climate perturbations: A single-LES exploration extending the
446 CGILS cases. *Journal of Advances in Modeling Earth Systems*, *5*(2), 316–337.
447 https://doi.org/10.1002/jame.20019

448 Brient, F., Roehrig, R., & Voldoire, A. (2019). Evaluating Marine Stratocumulus Clouds in the
449 CNRM-CM6-1 Model Using Short-Term Hindcasts. *Journal of Advances in Modeling*
450 *Earth Systems*, *11*(1), 127–148. https://doi.org/10.1029/2018MS001461

451 Burnet, F., & Brenguier, J. L. (2007). Observational study of the entrainment-mixing process in
452 warm convective clouds. *Journal of the Atmospheric Sciences*, *64*(6), 1995–2011.
453 https://doi.org/10.1175/JAS3928.1

454 Caldwell, P. M., & Bretherton, C. S. (2009). Response of a subtropical stratocumulus-capped
455 mixed layer to climate and aerosol changes. *Journal of Climate*, *22*(1), 20–38.
456 https://doi.org/10.1175/2008JCLI1967.1

457 Caldwell, P. M., Zhang, Y., Klein, S. A., Caldwell, P. M., Zhang, Y., & Klein, S. A. (2013).
458 CMIP3 subtropical stratocumulus cloud feedback interpreted through a mixed-layer model.
459 *Journal of Climate*, *26*(5), 1607–1625. https://doi.org/10.1175/JCLI-D-12-00188.1

460 Calmer, R., Roberts, G. C., Sanchez, K. J., Sciare, J., Sellegri, K., Picard, D., et al. (2019).
461 Aerosol Cloud Closure Study on Cloud Optical Properties using Remotely Piloted Aircraft
462 Measurements during a BACCHUS Field Campaign in Cyprus. *Atmospheric Chemistry and*
463 *Physics Discussions*, 1–35. https://doi.org/10.5194/acp-2019-8

464 Chen, Y.-C., Xue, L., Lebo, Z. J., Wang, H., Rasmussen, R. M., & Seinfeld, J. H. (2011).
465 Atmospheric Chemistry and Physics A comprehensive numerical study of aerosol-cloud-
466 precipitation interactions in marine stratocumulus. *Atmos. Chem. Phys*, *11*, 9749–9769.
467 https://doi.org/10.5194/acp-11-9749-2011

468 Chin, H. N. S., Rodriguez, D. J., Cederwall, R. T., Chuang, C. C., Grossman, A. S., Yio, J. J., et
469 al. (2000). A microphysical retrieval scheme for continental low-level stratiform clouds:
470 Impacts of the subadiabatic character on microphysical properties and radiation budgets.
471 *Monthly Weather Review*, *128*(7 II), 2511–2527. https://doi.org/10.1175/1520-
472 0493(2000)128<2511:amrsfc>2.0.co;2

473 Deardorff, J. W. (1980). Stratocumulus-capped mixed layers derived from a three-dimensional
474 model. *Boundary-Layer Meteorology*, *18*(4), 495–527. https://doi.org/10.1007/BF00119502

475 Diao, M. (2020). VCSEL 25 Hz Water Vapor Data. Version 1.0. UCAR/NCAR - Earth
476 Observing Laboratory. https://doi.org/https://doi.org/10.26023/V925-2H41-SD0F

477 Downey, A., Jasper, J. D., Gras, J. J., & Whittlestone, S. (1990). Lower tropospheric transport
478 over the Southern Ocean. *Journal of Atmospheric Chemistry*, *11*(1), 43–68.
479 https://doi.org/10.1007/BF00053667

480 Feingold, G., Eberhard, W. L., Veron, D. E., & Previdi, M. (2003). First measurements of the

Twomey indirect effect using ground-based remote sensors. *Geophysical Research Letters*, *30*(6). https://doi.org/10.1029/2002gl016633

Feingold, G., McComiskey, A., Rosenfeld, D., & Sorooshian, A. (2013). On the relationship between cloud contact time and precipitation susceptibility to aerosol. *Journal of Geophysical Research-Atmospheres*, *118*(18), 10544–10554. https://doi.org/10.1002/jgrd.50819

Geresdi, I., Meszaros, E., & Molnar, A. (2006). The effect of chemical composition and size distribution of aerosol particles on droplet formation and albedo of stratocumulus clouds. *Atmospheric Environment*, *40*(10), 1845–1855. https://doi.org/10.1016/j.atmosenv.2005.11.012

Grabowski, W. W. (1993). Cumulus entrainment, fine-scale mixing, and buoyancy reversal. *Quarterly Journal of the Royal Meteorological Society*, *119*(513), 935–956. https://doi.org/10.1002/qj.49711951305

Guo, H., Golaz, J. C., Donner, L. J., Larson, V. E., Schanen, D. P., & Griffin, B. M. (2010). Multi-variate probability density functions with dynamics for cloud droplet activation in large-scale models: Single column tests. *Geoscientific Model Development*, *3*(2), 475–486. https://doi.org/10.5194/gmd-3-475-2010

Guo, H., Golaz, J. C., Donner, L. J., Ginoux, P., & Hemler, R. S. (2014). Multivariate probability density functions with dynamics in the GFDL atmospheric general circulation Model: Global tests. *Journal of Climate*, *27*(5), 2087–2108. https://doi.org/10.1175/JCLI-D-13-00347.1

Hansen, J. E., & Travis, L. D. (1974). Light-Scattering in Planetary Atmospheres. *Space Science Reviews*, *16*(4), 527–610. https://doi.org/10.1007/bf00168069

Haynes, J. M., Jakob, C., Rossow, W. B., Tselioudis, G., Brown, J., Haynes, J. M., et al. (2011). Major Characteristics of Southern Ocean Cloud Regimes and Their Effects on the Energy Budget. *Journal of Climate*, *24*(19), 5061–5080. https://doi.org/10.1175/2011JCLI4052.1

Hill, A. A., Feingold, G., & Jiang, H. (2009). The influence of entrainment and mixing

assumption on aerosol-cloud interactions in marine stratocumulus. *Journal of the Atmospheric Sciences*, *66*(5), 1450–1464. https://doi.org/10.1175/2008JAS2909.1

Hourdin, F., Gəinusə-Bogdan, A., Braconnot, P., Dufresne, J. L., Traore, A. K., & Rio, C. (2015). Air moisture control on ocean surface temperature, hidden key to the warm bias enigma. *Geophysical Research Letters*, *42*(24), 10885–10893. https://doi.org/10.1002/2015GL066764

Hyder, P., Edwards, J. M., Allan, R. P., Hewitt, H. T., Bracegirdle, T. J., Gregory, J. M., et al. (2018). Critical Southern Ocean climate model biases traced to atmospheric model cloud errors. *Nature Communications*, *9*(1). https://doi.org/10.1038/s41467-018-05634-2

IPCC. (2014). *Climate Change 2014: Impacts, Adaptation, and Vulnerability. Part A: Global and Sectoral Aspects. Contribution of Working Group II to the Fifth Assessment Report of the Intergovernmental Panel on Climate Change [Field, C.B., V.R. Barros, D.J. Dokken, K.J.* Cambridge, United Kingdom and New York, NY, USA: Cambridge University Press.

Jacobson, M. Z., Turco, R. P., Jensen, E. J., & Toon, O. B. (1994). Modeling Coagulation Among Particles of Different Composition and Size. *Atmospheric Environment*, *28*(7), 1327–1338. https://doi.org/10.1016/1352-2310(94)90280-1

Jia, H., Ma, X., & Liu, Y. (2019). Exploring aerosol cloud interaction using VOCALS-REx aircraft measurements. *Atmospheric Chemistry and Physics Discussions*, *3*, 1–26. https://doi.org/10.5194/acp-2018-667

Jiang, H., Xue, H., Teller, A., Feingold, G., & Levin, Z. (2006). Aerosol effects on the lifetime of shallow cumulus. *Geophysical Research Letters*, *33*(14), 2–5. https://doi.org/10.1029/2006GL026024

Kato, S., Mace, G. G., Clothiaux, E. E., Liljegren, J. C., & Austin, R. T. (2001). Doppler cloud radar derived drop size distributions in liquid water stratus clouds. *Journal of the Atmospheric Sciences*, *58*(19), 2895–2911. https://doi.org/10.1175/1520-0469(2001)058<2895:DCRDDS>2.0.CO;2

Kogan, Z. N., Mechem, D. B., & Kogan, Y. L. (2005). Assessment of variability in continental

low stratiform clouds based on observations of radar reflectivity. *Journal of Geophysical Research D: Atmospheres*, *110*(18), 1–15. https://doi.org/10.1029/2005JD006158

Kohler, H. (1936). The nucleus in and the growth of hygroscopic droplets. *Transactions of the Faraday Society*, *32*(2), 1152–1161. https://doi.org/10.1039/tf9363201152

Laursen, K. K., Jorgensen, D. P., Brasseur, G. P., Ustin, S. L., & Huning, J. R. (2006). Hiaper: The next generation NSF/NCAR research aircraft. *Bulletin of the American Meteorological Society*, *87*(7), 896–909. https://doi.org/10.1175/BAMS-87-7-896

Lenschow, D. H., Krummel, P. B., & Siems, S. T. (1999). Measuring entrainment, divergence, and vorticity on the mesoscale from aircraft. *Journal of Atmospheric and Oceanic Technology*, *16*(10), 1384–1400. https://doi.org/10.1175/1520-0426(1999)016<1384:medavo>2.0.co;2

Lohmann, U. (2017). Anthropogenic Aerosol Influences on Mixed-Phase Clouds. *Current Climate Change Reports*, *3*(1), 32–44. https://doi.org/10.1007/s40641-017-0059-9

Lu, M. L., & Seinfeld, J. H. (2005). Study of the aerosol indirect effect by large-eddy simulation of marine stratocumulus. *Journal of the Atmospheric Sciences*, *62*(11), 3909–3932. https://doi.org/10.1175/JAS3584.1

Lu, M. L., Feingold, G., Jonsson, H. H., Chuang, P. Y., Gates, H., Flagan, R. C., & Seinfeld, J. H. (2008). Aerosol-cloud relationships in continental shallow cumulus. *Journal of Geophysical Research Atmospheres*, *113*(15), 1–21. https://doi.org/10.1029/2007JD009354

Martin, G. M., Johnson, D. W., & Spice, A. (1994). The Measurement and Parameterization of Effective Radius of Droplets in Warm Stratocumulus Clouds. *Journal of the Atmospheric Sciences*. https://doi.org/10.1175/1520-0469(1994)051<1823:tmapoe>2.0.co;2

Mason, S., Fletcher, J. K., Haynes, J. M., Franklin, C., Protat, A., Jakob, C., et al. (2015). A Hybrid Cloud Regime Methodology Used to Evaluate Southern Ocean Cloud and Shortwave Radiation Errors in ACCESS. *Journal of Climate*, *28*(15), 6001–6018. https://doi.org/10.1175/JCLI-D-14-00846.1

McCoy, D. T., Hartmann, D. L., Grosvenor, D. P., McCoy, D. T., Hartmann, D. L., &

562 Grosvenor, D. P. (2014). Observed Southern Ocean Cloud Properties and Shortwave
563 Reflection. Part I: Calculation of SW Flux from Observed Cloud Properties*. *Journal of*
564 *Climate*, *27*(23), 8836–8857. https://doi.org/10.1175/JCLI-D-14-00287.1

565 Nazarenko, L., Rind, D., Tsigaridis, K., Del Genio, A. D., Kelley, M., & Tausnev, N. (2017).
566 Interactive nature of climate change and aerosol forcing. *Journal of Geophysical Research*,
567 *122*(6), 3457–3480. https://doi.org/10.1002/2016JD025809

568 Paluch, I. R. (1979). Entrainment Mechanism in Colorado Cumuli. *Journal of the Atmospheric*
569 *Sciences*, *36*(12), 2467–2478. https://doi.org/10.1175/1520-
570 0469(1979)036<2467:temicc>2.0.co;2

571 Petters, M. D., & Kreidenweis, S. M. (2007). A single parameter representation of hygroscopic
572 growth and cloud condensation nucleus activity. *Atmospheric Chemistry and Physics*, *13*(2),
573 1081–1091. https://doi.org/10.5194/acp-13-1081-2013

574 Qu, X., Hall, A., Klein, S. A., & Caldwell, P. M. (2015). The strength of the tropical inversion
575 and its response to climate change in 18 CMIP5 models. *Climate Dynamics*, *45*(1–2), 375–
576 396. https://doi.org/10.1007/s00382-014-2441-9

577 Raatikainen, T., Nenes, A., Seinfeld, J. H., Morales, R., Moore, R. H., Lathem, T. L., et al.
578 (2013). Worldwide data sets constrain the water vapor uptake coefficient in cloud
579 formation. *Proceedings of the National Academy of Sciences of the United States of*
580 *America*, *110*(10), 3760–3764. https://doi.org/10.1073/pnas.1219591110

581 Rauber, R. M., Stevens, B., Ochs, H. T., Knight, C., Albrecht, B. A., Blyth, A. M., et al. (2007).
582 Rain in Shallow Cumulus Over the Ocean: The RICO Campaign. *Bulletin of the American*
583 *Meteorological Society*, *88*(12), 1912–1928. https://doi.org/10.1175/BAMS-88-12-1912

584 Reutter, P., Su, H., Trentmann, J., Simmel, M., Rose, D., Gunthe, S. S., et al. (2009). Aerosol-
585 and updraft-limited regimes of cloud droplet formation: influence of particle number, size
586 and hygroscopicity on the activation of cloud condensation nuclei (CCN). *Atmospheric*
587 *Chemistry and Physics*, *9*(18), 7067–7080. Retrieved from %3CGo

588 Roberts, G. C., & Nenes, A. (2005). A continuous-flow streamwise thermal-gradient CCN

589 chamber for atmospheric measurements. *Aerosol Science and Technology*, *39*(3), 206–221.
590 https://doi.org/10.1080/027868290913988

591 Roberts, G. C., Ramana, M. V, Corrigan, C., Kim, D., & Ramanathan, V. (2008). Simultaneous
592 observations of aerosol-cloud-albedo interactions with three stacked unmanned aerial
593 vehicles. *Proceedings of the National Academy of Sciences of the United States of America*,
594 *105*(21), 7370–7375. https://doi.org/10.1073/pnas.0710308105

595 Rosenfeld, D., Zheng, Y., Hashimshoni, E., Pöhlker, M. L., Jefferson, A., Pöhlker, C., et al.
596 (2016). Satellite retrieval of cloud condensation nuclei concentrations by using clouds as
597 CCN chambers. *Proceedings of the National Academy of Sciences*, *113*(21), 5828–5834.
598 https://doi.org/10.1073/pnas.1514044113

599 Russell, L. M., & Seinfeld, J. H. (1998). Size- and Composition-Resolved Externally Mixed
600 Aerosol Model. *Aerosol Science and Technology*, *28*(5), 403–416.
601 https://doi.org/10.1080/02786829808965534

602 Russell, L. M., Lenschow, D. H., Laursen, K. K., Krummel, P. B., Siems, S. T., Bandy, A. R., et
603 al. (1998). Bidirectional mixing in an ACE 1 marine boundary layer overlain by a second
604 turbulent layer. *Journal of Geophysical Research Atmospheres*, *103*(D13), 16411–16432.
605 https://doi.org/10.1029/97JD03437

606 Russell, L. M., Seinfeld, J. H., Flagan, R. C., Ferek, R. J., Hegg, D. A., Hobbs, P. V., et al.
607 (1999). Aerosol dynamics in ship tracks. *Journal of Geophysical Research Atmospheres*,
608 *104*(D24), 31077–31095. https://doi.org/10.1029/1999JD900985

609 Sanchez, K. J., & Roberts, G. C. (2018). SOCRATES CCN measurements. Version 1.1.
610 UCAR/NCAR - Earth Observing Laboratory. https://doi.org/10.5065/D6Z036XB

611 Sanchez, K. J., Russell, L. M., Modini, R. L., Frossard, A. A., Ahlm, L., Corrigan, C. E., et al.
612 (2016). Meteorological and aerosol effects on marine cloud microphysical properties.
613 *Journal of Geophysical Research*, *121*(8), 4142–4161.
614 https://doi.org/10.1002/2015JD024595

615 Sanchez, K. J., Roberts, G. C., Calmer, R., Nicoll, K., Hashimshoni, E., Rosenfeld, D., et al.

(2017). Top-down and Bottom-up aerosol-cloud-closure: towards understanding sources of uncertainty in deriving cloud radiative flux. *Atmospheric Chemistry and Physics Discussions*, *17*(March), 1–32. https://doi.org/10.5194/acp-2017-201

Schnaiter, M., Järvinen, E., Abdelmonem, A., & Leisner, T. (2018). PHIPS-HALO: The airborne particle habit imaging and polar scattering probe - Part 2: Characterization and first results. *Atmospheric Measurement Techniques*, *11*(1), 341–357. https://doi.org/10.5194/amt-11-341-2018

Seinfeld, J. H., & Pandis, S. N. (2006). *Atmospheric Chemistry and Physics: From Air Pollution to Climate Change*. New York: Wiley. Retrieved from https://books.google.com/books?id=tZEpAQAAMAAJ

Seinfeld, J. H., Bretherton, C. S., Carslaw, K. S., Coe, H., DeMott, P. J., Dunlea, E. J., et al. (2016). Improving our fundamental understanding of the role of aerosol-cloud interactions in the climate system. *Proceedings of the National Academy of Sciences of the United States of America*, *113*(21), 5781–90. https://doi.org/10.1073/pnas.1514043113

Stephens, G. L. (1978). Radiation Profiles in Extended Water Clouds 2. Parameterization Schemes. *Journal of the Atmospheric Sciences*, *35*(11), 2123–2132. https://doi.org/10.1175/1520-0469(1978)035<2123:rpiewc>2.0.co;2

Stevens, B. (2002). Entrainment in stratocumulus-topped mixed layers. *Quarterly Journal of the Royal Meteorological Society*, *128*(586 PART B), 2663–2690. https://doi.org/10.1256/qj.01.202

Stevens, B. (2015). Rethinking the lower bound on aerosol radiative forcing. *Journal of Climate*, *28*(12), 4794–4819. https://doi.org/10.1175/JCLI-D-14-00656.1

Stevens, B., Moeng, C. H., Ackerman, A. S., Bretherton, C. S., Chlond, A., de Roode, S., et al. (2005). Evaluation of large-eddy simulations via observations of nocturnal marine stratocumulus. *Monthly Weather Review*, *133*(6), 1443–1462. https://doi.org/10.1175/MWR2930.1

de Szoeke, S. P., Fairall, C. W., Wolfe, D. E., Bariteau, L., & Zuidema, P. (2010). Surface flux

observations on the southeastern tropical pacific ocean and attribution of sst errors in coupled ocean-atmosphere models. *Journal of Climate*, *23*(15), 4152–4174. https://doi.org/10.1175/2010JCLI3411.1

Turton, J. D., & Nicholls, S. (1987). A Study of the Diurnal-Variation of Stratocumulus Using a Multiple Mixed Layer Model. *Quarterly Journal of the Royal Meteorological Society*, *113*(477), 969–1009. https://doi.org/10.1256/smsqj.47710

Twomey, S. (1977). The Influence of Pollution on the Shortwave Albedo of Clouds. *Journal of the Atmospheric Sciences*, *34*(7), 1149–1152. https://doi.org/10.1175/1520-0469(1977)034<1149:TIOPOT>2.0.CO;2

Tzivion, S., Feingold, G., & Levin, Z. (1987). An efficient numerical solution to the stochastic collection equation. *Journal of the Atmospheric Sciences*, *44*(21), 3139–3149. https://doi.org/10.1175/1520-0469(1987)044<3139:aenstt>2.0.co;2

UCAR/NCAR-Earth Observing Laboratory. (2018). NCAR HCR radar moments data. Version 1.0. UCAR/NCAR - Earth Observing Laboratory. https://doi.org/10.5065/D68914PH

UCAR/NCAR-Earth Observing Laboratory. (2019a). High Rate (HRT - 25 sps) Navigation, State Parameter, and Microphysics Flight-Level Data. Version 1.0. UCAR/NCAR - Earth Observing Laboratory. https://doi.org/.26023/K5VQ-K6KY-W610

UCAR/NCAR-Earth Observing Laboratory. (2019b). Low Rate (LRT - 1 sps) Navigation, State Parameter, and Microphysics Flight-Level Data. Version 1.3. UCAR/NCAR - Earth Observing Laboratory. https://doi.org/10.5065/D6M32TM9

Vial, J., Dufresne, J. L., & Bony, S. (2013). On the interpretation of inter-model spread in CMIP5 climate sensitivity estimates. *Climate Dynamics*, *41*(11–12), 3339–3362. https://doi.org/10.1007/s00382-013-1725-9

Wang, M., Ghan, S., Liu, X., L'Ecuyer, T. S., Zhang, K., Morrison, H., et al. (2012). Constraining cloud lifetime effects of aerosols using A-Train satellite observations. *Geophysical Research Letters*, *39*(15), 3–9. https://doi.org/10.1029/2012GL052204

Wang, S., Wang, Q., & Feingold, G. (2003). Turbulence, condensation, and liquid water

transport in numerically simulated nonprecipitating stratocumulus clouds. *Journal of the Atmospheric Sciences*, *60*(2), 262–278. https://doi.org/10.1175/1520-0469(2003)060<0262:TCALWT>2.0.CO;2

Webb, M. J., & Lock, A. P. (2013). Coupling between subtropical cloud feedback and the local hydrological cycle in a climate model. *Climate Dynamics*, *41*(7–8), 1923–1939. https://doi.org/10.1007/s00382-012-1608-5

Whittlestone, S., & Zahorowski, W. (1998). Baseline radon detectors for shipboard use: Development and deployment in the First Aerosol Characterization Experiment (ACE 1). *Journal of Geophysical Research-Atmospheres*, *103*(D13), 16743–16751. https://doi.org/10.1029/98jd00687

Wood, R. (2007). Cancellation of Aerosol Indirect Effects in Marine Stratocumulus through Cloud Thinning. *Journal of the Atmospheric Sciences*, *64*(7), 2657–2669. https://doi.org/10.1175/JAS3942.1

Xue, H., & Feingold, G. (2006). Large-eddy simulations of trade wind cumuli: Investigation of aerosol indirect effects. *Journal of the Atmospheric Sciences*, *63*(6), 1605–1622. https://doi.org/10.1175/JAS3706.1

Yum, S. S., Hudson, J. G., & Xie, Y. (1998). *Comparisons of cloud microphysics with cloud condensation nuclei spectra over the summertime Southern Ocean*. *Journal of Geophysical Research Atmospheres* (Vol. 103). https://doi.org/10.1029/98JD01513

Zondlo, M. A., Paige, M. E., Massick, S. M., & Silver, J. A. (2010). Vertical cavity laser hygrometer for the National Science Foundation Gulfstream-V aircraft. *Journal of Geophysical Research Atmospheres*, *115*(20), 1–14. https://doi.org/10.1029/2010JD014445

Zuidema, P., Xue, H., & Feingold, G. (2008). Shortwave radiative impacts from aerosol effects on marine shallow cumuli. *Journal of the Atmospheric Sciences*, *65*(6), 1979–1990. https://doi.org/10.1175/2007JAS2447.1

696

697 **Figure 1**. The measurement derived q_v and θ_E for the RF12 (a) and RF10$_{Thick}$ (b) cases. The in-
698 cloud fit is the in-cloud q_v and θ_E calculated from linear fits of the temperature and pressure
699 vertical profiles with the assumption that in-cloud RH$_{liq}$ = 100%. The above cloud measurements
700 with red circles are the measurements that are used in the calculation to correct for the effect of
701 entrainment on the cloud microphysical and optical properties (See Supporting text S3 and S4 for
702 identifying entrained air properties and calculation details). The measurements marked as
703 entrained air are considered to be representative of the air properties that are entrained into the
704 cloud. The black solid and dashed lines are mixing lines connecting the cloud base properties to
705 three of the entrained air points and represent the expected total water content as a function of θ_E.
706 The mixing lines shown represent the median and 25th, 75th percentiles in LWC and CDNC
707 derived from all mixing lines and correspond to calculated LWC and CDNC profiles shown in
708 Figure 2. Similar plots for RF02, RF10$_{Thin}$ and RF13 are shown in Supporting Figure S4.

709 **Figure 2.** Observed and simulated cloud properties for the RF12 (a-d) and RF10$_{Thick}$ (e-h) case.
710 The observed properties were obtained from the CDP measurements, except for the extinction,
711 which was calculated from the observed CDP distributions. The ENT$_{LWC}$ and ENT$_{ML}$ D$_v$ profile
712 is identical to the adiabatic profile due to the assumption of inhomogeneous entrainment. By
713 definition, the LWC for ENT$_{LWC}$ is the same as what was observed so there is no ENT$_{LWC}$ line
714 on the LWC profile. The ENT$_{ML}$ profile is dependent on the properties of the entrained air (red
715 circles in Figure 2). The solid black line is the median LWC and CDNC from the distribution of
716 profiles derived from the ENT$_{ML}$ analysis (Section 2.5) and the dashed lines represent the 25th
717 and 75th percentiles and correspond to the mixing lines shown in Figure 1. Vertical profiles for
718 RF02, RF10$_{Thin}$ and RF13 are shown in Supporting Figure S5.

Table 1. GV observed below-cloud aerosol concentrations, in-cloud droplet properties and calculated optical properties. ACPM simulation results are present for adiabatic simulations, as well as simulations for LWC entrainment method and mixing line entrainment method. The sensitivity of below-cloud particle number concentration, updraft velocity and cloud LWP (which is affected by cloud-top entrainment) on SWCF and CDNC. Sensitivities for SWCF are calculated for both the adiabatic (ENT_{LWC}) simulations. Sensitivities for CDNC are the same for adiabatic simulations and ENT_{LWC}.

	RF02	**RF10$_{Thin}$**	**RF10$_{Thick}$**	**RF12**	**RF13**
Observed					
$CDNC_{obs}$ (cm^{-3})	64±11	97±17	94±51	175±34	143±24
$SWCF_{obs}$ ($W\ m^{-2}$)	103.1	142.9	340.1	234.3	201.1
Droplet spectra width[a]	0.81±0.04	0.84±0.03	0.73±0.12	0.82±0.05	0.83±0.05
Max LWC ($g\ m^{-3}$)	0.23	0.30	0.68	0.40	0.36
LWP ($g\ m^{-2}$)[b]	1.29	2.02	19.89	6.47	3.94
Below cloud Aerosol (cm^{-3})	457±9	463±62	956±17	505±52	290±66
Below cloud Aerosol (>70 nm, cm^{-3})	161±42	167±29	193±45	269±74	199±38
Cloud base height (m)	500	1010	290	1090	790
Cloud top height (m)	660	1210	870	1450	1030
Cloud base temperature (K)	274.9	273.3	283.9	268.3	274.3
Cloud top temperature (K)	273.9	272.1	281.1	265.7	272.6
Simulations					
	Adiabatic				
$CDNC_{adiabatic}$ (cm^{-3})	176	198	226	286	220
$SWCF_{adiabatic}$ ($W\ m^{-2}$)[c]	196.5±17.1	220.8±16.5	387.3±9.4	272.7±8.9	242.2±7.0
Droplet spectra width	0.96	0.97	0.91	0.96	0.97
Max LWC ($g\ m^{-3}$)	0.32	0.38	1.59	0.55	0.47
LWP ($g\ m^{-2}$)	2.34	3.61	47.31	9.79	5.48
TOA incoming solar radiation ($W\ m^{-2}$)	453.8	419.4	431.3	365.7	393.2
	LWC Entrainment (ENT_{LWC})				
$CDNC_{ENT_{LWC}}$ (cm^{-3})	97±24	109±40	115±60	188±18	156±21
$SWCF_{ENT_{LWC}}$ ($W\ m^{-2}$)[c]	135.2±14.2	158.8±15.2	345.4±16.2	242.7±10.4	212.5±7.3
Entrainment reduction in adiabatic LWP	45%	44%	**58%**	34%	**28%**
SWCF for **28%** and **58%** reduction from adiabatic LWP ($W\ m^{-2}$)	161.0, 110.2	186.4, 133.5	372.6, 339.6	248.1, 201.8	210.7, 158.3
	Mixing Line Entrainment (ENT_{ML}; Sanchez et al. 2017)[d]				
$CDNC_{ENT_{ML}}$ (cm^{-3}) 50th percentile	79±10	160±5	166±65	151±20	132±19
25th and 75th percentiles	17.7-103	127-176	161-172	134-191	109-220
$SWCF_{ENT_{ML}}$ ($W\ m^{-2}$) 50th percentile	102.2±12.1	197.1±16.2	367.7±12.8	220.5±11.0	189.3±7.6
25th and 75th percentiles	27.2-128.6	172.9-207.9	365.4-370.6	220.5-241.1	170.7-242.2
	Difference between simulated and observed SWCF[c]				
$\delta SWCF_{adiabatic}$	93.4±17.1	77.9±16.5	47.2±9.4	38.4±8.9	41.1±7.0
$\delta SWCF_{ENT_{LWC}}$	32.1±14.2	15.9±15.2	5.3±16.2	8.4±10.4	11.4±7.3
$\delta SWCF_{ENT_{ML}}$	-0.9±12.1	54.2±16.2	27.6±12.8	-13.8±11.0	-11.8±7.6
Sensitivity Tests	**$S(X_i) = dln(Y_i)/dln(X_i)$ (Feingold et al., 2003)**				
X_i	**Y_i = SWCF**				
N_p	0.149 (0.145)	0.109 (0.130)	0.031 (0.059)	0.060 (0.088)	0.084 (0.090)
w	0.033 (0.034)	0.027 (0.042)	0.014 (0.027)	0.022 (0.033)	0.019 (0.021)
LWP	0.632	0.569	0.132	0.281	0.397
X_i	**$Y_i = CDNC_{avg}$**				
N_p	0.776	0.707	0.888	0.743	0.705
w	0.433	0.428	0.485	0.301	0.250
LWP	1.014	1.025	0.776	1.007	1.053

[a](Martin et al., 1994). [b]Liquid water path is calculated from CDP distribution profile. [c]The uncertainty includes the potential error of ± 20 % in updraft velocity (w) and the standard error of the CCN concentration measurements. [d]The 25th, 50th and 75th percentile in SWCF and CDNC obtained from the distribution of profiles generated by the ENT_{ML} analysis (Section 2.5, Figure 1,2).

Figure1.

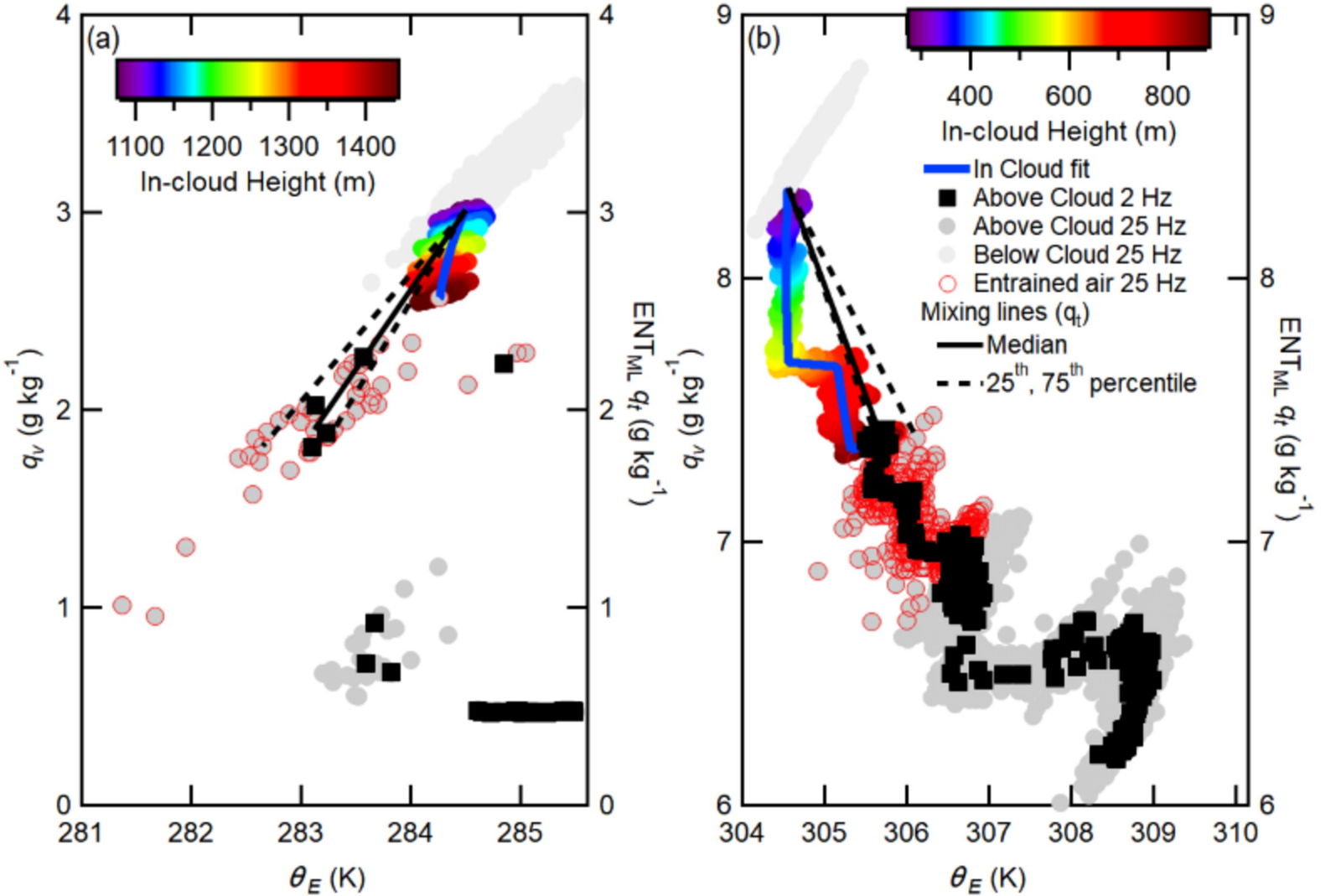
(a)
1100 1200 1300 1400
In-cloud Height (m)
q_v (g kg^{-1})
ENT_{ML} q_t (g kg^{-1})
θ_E (K)
(b)
400 600 800
In-cloud Height (m)
In Cloud fit
Above Cloud 2 Hz
Above Cloud 25 Hz
Below Cloud 25 Hz
Entrained air 25 Hz
Mixing lines (q_t)
Median
25th, 75th percentile
q_t (g kg^{-1})
ENT_{ML} q_t (g kg^{-1})
θ_E (K)

Figure2.

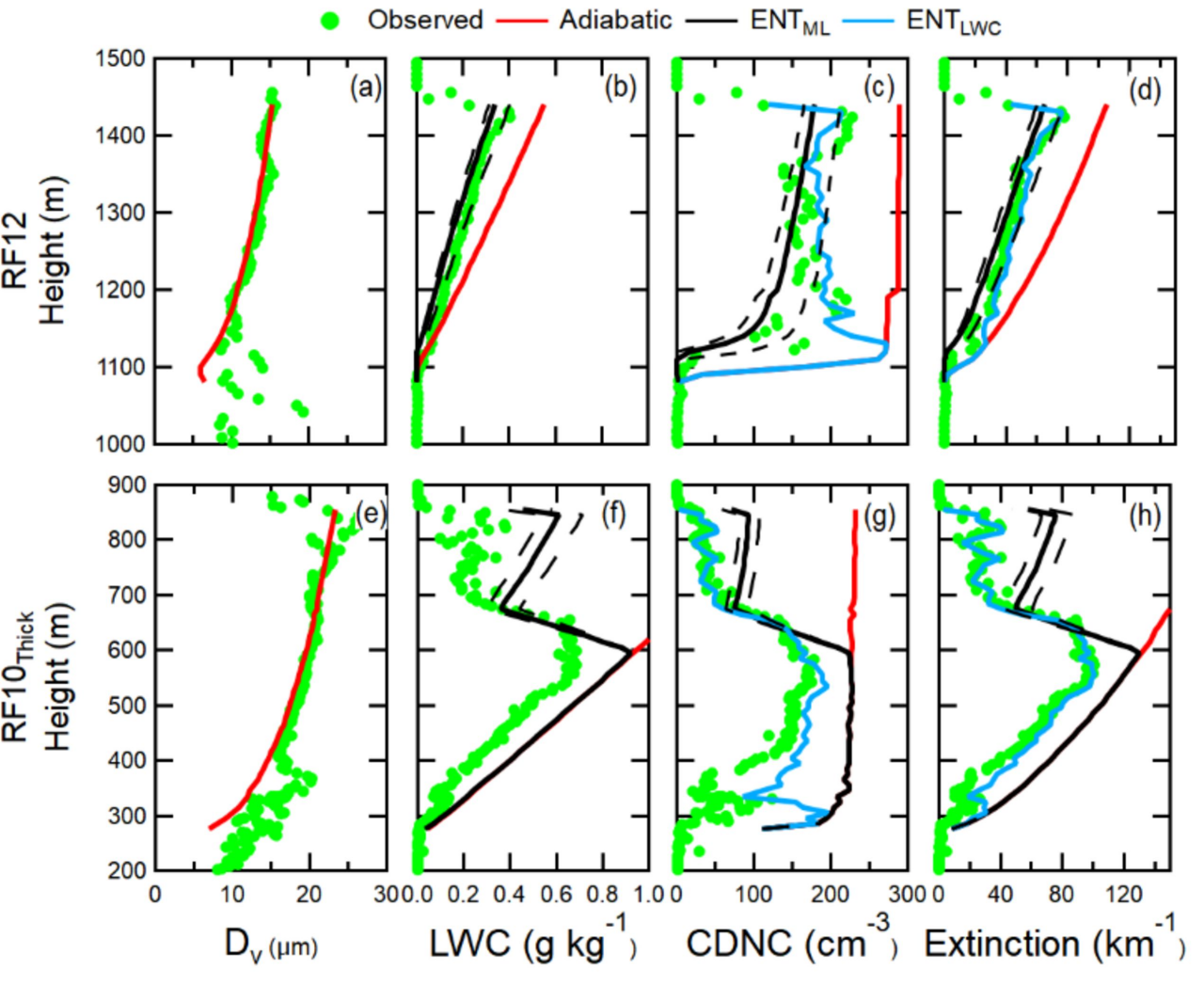
Observed
Adiabatic
ENT$_{ML}$
ENT$_{LWC}$
RF12
Height (m)
RF10$_{Thick}$
Height (m)
(a)
(b)
(c)
(d)
(e)
(f)
(g)
(h)
1500
1400
1300
1200
1100
1000
900
800
700
600
500
400
300
200
0
10
20
30
0.0
0.2
0.4
0.6
0.8
1.0
0
100
200
300
0
40
80
120
D_v (μm)
LWC (g kg^{-1})
CDNC (cm^{-3})
Extinction (km^{-1})